Received: 9 April 2021 | Revised: 4 August 2021 | Accepted: 22 August 2021

DOI: 10.1002/jbm.b.34930

RESEARCH ARTICLE

Society For Biomaterials | WILEY

Mechanical properties and *in vitro* bioactivity of silicon nitride ceramics with SiO_2, CaO, and MgO additions

Celso Ricardo Sona Filho[1] | **Flávio Machado de Souza Carvalho**[2] | **Cecilia Chaves Guedes-Silva**[1]

[1]Instituto de Pesquisas Energéticas e Nucleares, IPEN–CNEN/SP, São Paulo, SP, Brazil

[2]Departamento de Mineralogia e Geotectônica, Instituto de Geociências, Universidade de São Paulo, USP, SP, Brazil

Correspondence
Cecilia Chaves Guedes-Silva, Instituto de Pesquisas Energéticas e Nucleares, IPEN–CNEN/SP, São Paulo, SP, 05508-000, Brazil.
Email: cecilia.guedes@ipen.br

Funding information
Fundação de Amparo à Pesquisa do Estado de São Paulo, Grant/Award Number: 2015/02265-7

Abstract

Silicon nitride ceramics with SiO_2, CaO, and MgO as sintering aids were investigated in view of biomedical applications. In the current study, samples with four different compositions were pressureless sintered at 1750°C for 1 h under a nitrogen atmosphere. The samples were evaluated concerning densification, microstructure, mechanical properties, and *in vitro* bioactivity. Microstructures with elongated β-Si_3N_4 grains dispersed in an intergranular phase and with densities from 78.77 to 97.14% of the theoretical density were obtained. Higher contents of SiO_2 resulted in the best densification and mechanical properties. Besides, replacements of CaO by MgO in the initial compositions affected Young's modulus and *in vitro* bioactivity. Considering the samples with relative density higher than 94.14%, those with lower values of Young's modulus had lower SiO_2/MgO ratios. After immersion in SBF (Simulated Body Fluid), the samples with high porosity and/or partial replacements of CaO by MgO had their surfaces coated with a layer rich in calcium and phosphorus, morphologically similar to hydroxyapatite. Hence, producing silicon nitride ceramics with the potential to be used as orthopedic implants must consider ideal amounts of additives. In this article, the best combination of mechanical properties and mineralization capability was reached by the composition with low content of MgO, and high content of SiO_2 and CaO.

KEYWORDS
bioceramics, mechanical properties, silicon nitride

1 | INTRODUCTION

Due to their excellent mechanical properties, noncytotoxicity, and osteointegration capacity, silicon nitride based ceramics have been widely considered for different applications in the medical field.[1-4] The success of their use as intervertebral spacers in spinal arthrodesis has encouraged researchers to carry out several studies to expand their application to other components and medical devices, such as hip prostheses as well as plates and pins for bone fixation. These studies address investigations on the tribological behavior of this ceramic, *in vitro* cellular response, antibacterial function, and production of porous parts for bone filling.[3-10]

However, as most clinical applications require bioactivity, that is, bonding between implanted material and neighboring tissue, bioinert materials such as silicon nitride have been combined with bioactive materials to induce specific biological activity. Hydroxyapatite coated silicon nitride based ceramics obtained by the biomimetic or sol-gel method, together with silicon nitride composites containing Bioglass and hydroxyapatite as a second phase, had the bioactivity demonstrated by the formation of a bone-like hydroxyapatite layer on their surfaces after immersions in SBF (Simulated Body Fluid).[11-13]

On the other hand, silicon nitride presents a low diffusion coefficient due to the covalent chemical bond, which becomes it challenging to be densified by solid-state diffusion. Thus, the material

densification should occur through liquid-phase sintering, which involves the addition of sintering aids. These additives remain in the material's grain boundaries and triple points as a secondary phase.[14]

The reaction of the sintering aids with SiO_2, which is always present on the surface of α-Si_3N_4 particles, promotes the solution/precipitation process followed by the $\alpha \rightarrow \beta$-Si_3N_4 transformation. Understanding the role of the sintering aids on the final properties of the material is essential because the intergranular secondary phase affects the final properties of the material.[15-17]

For structural applications at high temperatures, rare earth oxides have been highlighted as silicon nitride sintering aids. These oxides form a viscous liquid phase ables to promote the solution/precipitation process and be crystallized during the cooling step or after specific heat treatments.[18] However, besides promoting the liquid-phase sintering process, the used additives must result in an intergranular glassy phase with a proper biological response. Some therapeutic ion oxides such as Li^+, Sr^{2+}, Zn^{2+}, Ca^{2+}, Mg^{2+}, Cu^{2+}, Ti^{4+}, and Si^{4+}, able to stimulate tissue regeneration processes, can be efficient to produce silicon nitride bioceramics. Studies using SrO, MgO, and SiO_2 (together) as sintering aids of Si_3N_4 have shown that the simultaneous combination of these oxides results in materials with low bacterial affinity as well as good proliferation ability and differentiation potential of pre-osteoblasts cells.[18] Other researches[19,20] have evaluated the densification, mechanical properties, and *in vitro* biological behavior of silicon nitride ceramics containing SiO_2 and CaO with or without Al_2O_3 or TiO_2 as sintering aids. The results showed that the density of sintered materials, cell proliferation ability, and bioactivity in SBF can be improved depending on the amount of each oxide in the initial composition. However, in general, it was possible to obtain dense and bioactive silicon nitride ceramics suitable to stimulate *in vitro* cell growth.

Hence, the previous positive results found for silicon nitride bioceramics with $SiO_2 + CaO$, $SiO_2 + CaO + Al_2O_3$, $SiO_2 + TiO_2$, and $SiO_2 + SrO + MgO$ encouraged us to investigate new additives combinations with $SiO_2 + CaO + MgO$ and $SiO_2 + MgO$. The current article aims to understand the densification, mechanical properties, and *in vitro* bioactivity in SBF of silicon nitride containing therapeutic ion oxides (SiO_2, CaO, and MgO). During the implantation *in vivo*, the silicon introduction in the biomaterial stimulates bone mineralization around the implant.[21] At the same time, calcium can assist the osteoblast and osteoclast activity contributing to bone growth,[22] and finally, magnesium favors the adhesion and proliferation of osteoblastic cells.[23]

2 | MATERIALS AND METHODS

Commercial α-Si_3N_4 powder (UBE, SN-E10), MgO (periclase, Vetec, 94.12% purity), SiO_2 (quartz, 99.9% purity, Sigma-Aldrich), and $CaCO_3$ (P.A., Vetec) were used as starting powders. From properly weighed raw materials, four different compositions (designed as SN1, SN2, SN3, and SN4 in Table 1) were projected to have 20 wt. % additives and consequently form enough volume of intergranular phase to ensure the liquid sintering process and bioactivity. The amount of each oxide was selected to evaluate the effect of SiO_2 and CaO silicon nitride ceramics. All compositions were inspired by the good sintering and biological results found for samples with 12 wt. % SiO_2 and 8 wt. % CaO obtained in previous study.[19] Also, the amounts of MgO were selected considering the magnesium stored in tissues and organs, estimated at 5 mg/g.[24]

Hence, in SN1 and SN2 compositions, the content of SiO_2 was kept at 12 wt.%, while that of CaO was partially or entirely replaced by MgO. SN3 and SN4 were prepared to have 8 wt. % CaO while SiO_2 was partially replaced by MgO, resulting in a total amount of 12 wt.% ($MgO + SiO_2$). Next, the powders were ground in a ball mill for 24 h using isopropanol as the solvent and alumina balls as media. After drying at 90°C using a rotatory evaporator, the powders were compacted by uniaxial (50 MPa) and cold isostatic (200 MPa) pressing. Samples soaked in a powder bed of silicon nitride were pressureless sintering at 1750°C for 1 h using a graphite resistance furnace (Thermal Technology) in a high purity nitrogen atmosphere.

The apparent density and porosity of the sintered samples were determined using the Archimedes' method, using distilled water as the immersion liquid, while the relative density (RD) was determined considering the theoretical density estimable using the rule of mixture. After sintering, the crystalline phases were identified by X-ray powder diffraction (XRD; Bruker D8) with CuKα radiation. Microstructural observation of the samples was performed on the polished and plasma etched surfaces, using SF_6 and O_2, by scanning electron microscopy (SEM; PHILIPS—XL30).

The Young's modulus was determined by a nondestructive dynamic method (ASTM E 1876-15)[25] with the resonant frequency of the specimens measured in the flexion mode using the Grindosconic instrument. Flexural strengths of the ceramics were tested by three-point bending according to ASTM C1161-13,[26] while the hardness and fracture toughness were determined by the Vickers indentation method (Buhler VH1150 Durometer) with a load of 100 N. The lengths of the impression diagonals and surface cracks were measured so that the fracture toughness could be calculated using the equation of Anstis et al. (Equation 1)[27]:

$$K_{IC} = 0.016.\left(\left(\frac{E}{Hv}\right)^{1/2}\right).\frac{P}{c^{3/2}} \quad (1)$$

where K_{IC} is the fracture toughness, H_V is the Vickers hardness, E is Young's modulus, c is the half-length of radial crack, and P is the applied load.

To investigate the apatite mineralization and predict the bioactivity of the materials for potential application in clinical orthopedics, immersion testing of the sintered samples was performed in SBF with similar ion concentrations to human blood plasma. The samples were soaked at pH = 7.20, and 37°C with the solution exchanged every 60 h. After 2.5, 7.5, 14, and 24 days in SBF, the concentration of Ca^{2+}, Mg^{2+}, and P into the solution was analyzed by plasma-optical emission spectrometry (ICP-OES, Spectro ARCOS), and the samples

TABLE 1 Densification results and mechanical properties of the compositions studied in the current (*) and previous studies[19,20]

Composition	Porosity (%)	Apparent density (g/cm^3)	Relative density (%DT)	Vickers hardness (GPa)	Toughness fracture ($MPa.m^{1/2}$)	Young's modulus (GPa)	Flexural strength (MPa)
80wt%Si_3N_4 + 12wt%SiO_2 + 4wt%MgO + 4wt%CaO SN1*	2.38 ± 0.35	2.97 ± 0.06	94.88 ± 0.59	11.57 ± 0.29	6.83 ± 0.49	268.55 ± 5.57	569.01 ± 40.33
80wt%Si_3N_4 + 12wt%SiO_2 + 8wt%MgO SN2*	2.45 ± 0.88	3.05 ± 0.02	97.14 ± 2.19	11.70 ± 0.35	6.81 ± 0.64	259.75 ± 2.34	620.11 ± 54.23
80wt%Si_3N_4 + 8wt%SiO_2 + 4wt%MgO + 8wt%CaO SN3*	2.60 ± 0.39	2.99 ± 0.01	97.08 ± 1.94	9.34 ± 0.20	6.32 ± 0.37	252.78 ± 5.98	621.25 ± 61.81
80wt%Si_3N_4 + 4wt%SiO_2 + 8wt%MgO + 8wt%CaO SN4*	9.44 ± 0.97	2.52 ± 0.17	78.77 ± 0.04	8.98 ± 0.29	4.85 ± 0.17	132.28 ± 6.63	182.52 ± 25.82
80wt%Si_3N_4 + 12wt%SiO_2 + 8wt%CaO SSC-12[19]	–	3.00 ± 0.02	96.08 ± 0.69	11.71 ± 0.42	4.88 ± 0.52	269.80 ± 6.39	–
80wt%Si_3N_4 + 12wt%SiO_2 + 7.7wt%CaO + 0.3wt%Al_2O_3 SSC-12A[19]	–	3.01 ± 0.01	96.59 ± 0.37	11.07 ± 0.23	5.70 ± 0.55	271.63 ± 3.13	–
90wt%Si_3N_4 + 1wt%SiO_2 + 4wt%CaO + 5wt%TiO_2 SSCT-1[20]	0.32 ± 0.11	3.13 ± 0.01	97.56 ± 0.18	12.65 ± 0.30	6.48 ± 0.52	–	–
90wt%Si_3N_4 + 4wt%SiO_2 + 3.5wt%CaO + 2.5wt%TiO_2 SSCT-4[20]	0.93 ± 0.55	3.04 ± 0.02	96.32 ± 0.29	12.40 ± 0.32	5.52 ± 0.60	–	–

surfaces were observed by scanning electron microscopy (SEM, Hitachi TM-3000 SEM). High-resolution field-emission gun scanning electron microscopy and energy dispersive spectroscopy (FEG-SEM, JEOL JSM-6701F, and EDS, Thermo 6706C-3UUS-SN) were used to evaluate the samples surfaces after 24 days of immersion.

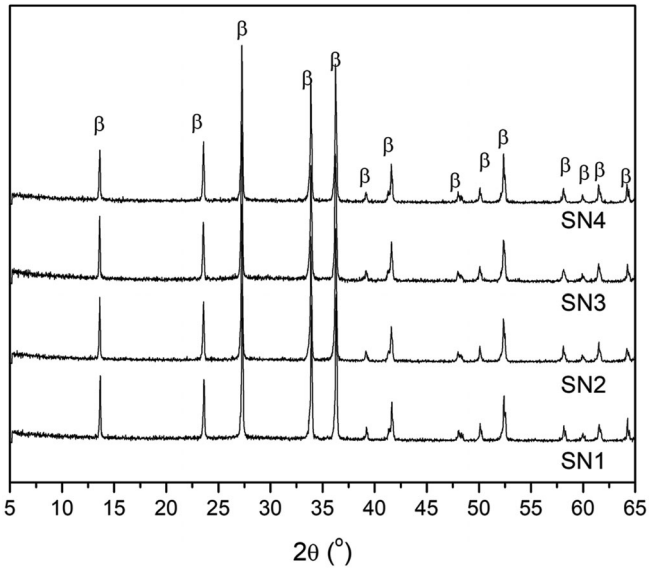

FIGURE 1 X-ray diffraction patterns of the silicon nitride samples (β is β-Si_3N_4)

3 | RESULTS AND DISCUSSION

The X-ray powder diffraction results of the sintered samples show that all compositions exhibited diffractograms (Figure 1) containing peaks of β-Si_3N_4 phase, exclusively. The exclusive presence of β-Si_3N_4 as a crystalline phase demonstrates that the sintering aids formed a liquid phase that could dissolve the α-Si_3N_4 particles, precipitated as β-Si_3N_4. After the cooling step, this liquid phase was kept in the material as glass, as related by.[28] The SEM images in Figure 2 illustrate the β-Si_3N_4 grains with a needle-like morphology dispersed in the secondary glassy phase. The needle-like β-Si_3N_4 grains are responsible for favoring the crack deflection toughening mechanism that, together with the composition of the intergranular glassy phase, improve the mechanical properties of the final material.[1,15]

Table 1 shows the values of density and apparent porosity of the current sintered samples and those studied in other works.[19,20] From this table, it is evident that SN1, SN2, and SN3 coded samples exhibited low values of porosity and high values of density, demonstrating that the amount and combination of additives as well as the sintering temperature of 1750°C were suitable to promote the

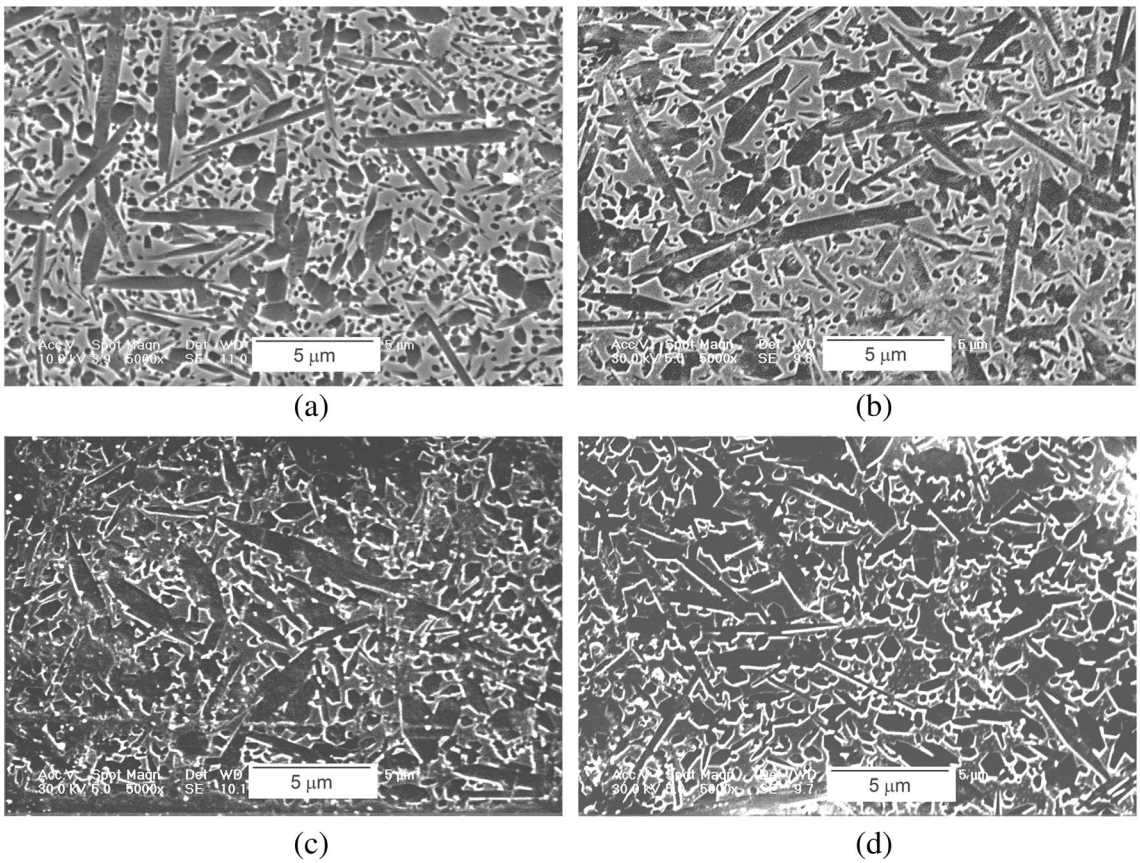

FIGURE 2 SEM images of (A) SN1, (B) SN2, (C) SN3, and (D) SN4 coded samples

pressureless liquid-phase sintering of silicon nitride. This successful sintering can be attributed to some factors such as the high content of silica presented in those compositions, which probably contributed to form a low viscous liquid phase at relatively low temperatures, from 1400 to 1600°C, according to the CaO–MgO–SiO_2 phase diagram described by Park et al.[29] Moreover, the highest value of relative density found for SN2 coded sample suggests that the density can be increased using compositions with higher contents of MgO besides SiO_2, probably because of changes in the liquid phase viscosity. The positive effect of MgO can be observed comparing the density of SN2 sample with those samples also containing CaO and SiO_2 but without MgO (SSC-12 and SSC-12A, Table 1[19]). It means that MgO additions may be more significant in the sintering process than the temperature since the samples studied before[19] were sintered at a higher temperature (1815°C) than that used in the present study (1750°C).

For Pedone et al.,[30] when CaO is replaced by MgO in the network of the 45S5 Bioglass, the melt viscosity is reduced due to the lower number of shared edges between MgO_5 and SiO_4 polyhedra in comparison to CaO_6-SiO_4 ones, which increases the number of larger rings in the silica matrix. On the other hand, the poor densification reached by SN4 sample, revealed by its high porosity and low density, can be related mainly to the very high liquid temperature of around 2200°C, also identified by analyzing the phase diagram of the CaO–MgO–SiO_2 system.[29]

The initial samples compositions influenced the hardness of silicon nitride samples because the additives composition affects the hardness of the glassy phase and the densification process, as earlier discussed. Comparing the results of SN1, SN2, SN3, and SN4 samples shown in Table 1, we can see that SN3 and SN4 reached values of hardness lower than those found for SN1 and SN2 samples as a consequence of the highest content of SiO_2. In addition, similar values of hardness were reached by SN1, SN2, SSC-12,[19] and SSC-12A[19] samples, containing the same content of silica as well as CaO and/or MgO.

Besides higher contents of SiO_2, the effect of the total content of the intergranular glassy phase on the hardness of the materials can be noticed by analyzing the data in Table 1. In general, silicon nitride ceramics with less glass are harder, as happened with samples with lower content of additives obtained in our previous study,[20] coded as SSCT-1 and SSCT-4. They presented increased values of hardness than all others with similar relative densities in Table 1 due to their composition characterized by a high content of Si_3N_4 (90 wt. %).

The hardness is critical for materials to be used in some biomedical applications because they are often accompanied by an increased wear resistance what minimizes the debris formation from the sliding between bone and implant surfaces. The presence of wear debris at the bone/implant interface is responsible for phenomena such as aseptic loosening and periprosthetic osteolysis, increasing the need for revision surgeries.[31]

Also, it is possible to observe from Table 1 that SN1, SN2, and SN3 coded samples presented higher fracture toughness, Young's modulus, and flexural strength than SN4 mainly because of their more significant densification. This behavior also suggests that the additives compositions with CaO, MgO, and high content of SiO_2 allowed obtaining silicon nitride ceramics with great mechanical performance, diminishing the risk of failure, therefore increasing the survival rate of orthopedic implants. We can observe from this table that the fracture toughness has been very close for SN1 and SN2 coded samples, and the values of around 6.8 MPa.$m^{1/2}$ were greater than that of 4.9 MPa.$m^{1/2}$ found for samples with similar compositions (designed as SSC-12 and SSC-12A in Reference 19), but without MgO. These results suggest that the presence of MgO tends to improve the fracture toughness of silicon nitride ceramics, probably because of replacements of Ca atoms by Mg in the glass network, which become structures with MgO more stable due to the higher bond energy of Mg-O than that of Ca–O.[32] Such behavior was very similar to that of Chen et al. [33] who found higher values of flexural strength and fracture toughness for the bioceramic of MgO–SiO_2–CaO system with the highest Mg/Ca molar ratio. Moreover, the results showed in Table 1 indicates that the presence of MgO in compositions containing CaO and high content of silica can increase the fracture toughness of silicon nitride ceramics to values higher than that reached by SSCT-1 and SSCT-4 samples, previously studied,[20] whose additions of TiO_2 promoted the formation of TiN as a reinforcement phase.

The data in Table 1 also shows that both densification and additives compositions influence on values of Young's modulus (E). The influence of porosity can be verified by the lowest Young's modulus found for sample SN4, with the highest porosity among all samples. As well as this, despite the presence of the strong Mg–O bonds in the glassy phase, it is possible to observe that E also tends to decline with increasing MgO. This behavior is showed comparing the results of samples with 12 wt. % SiO_2, that is, SN1, SN2, SSC-12[19] and SSC-12A.[19] Some works have also investigated the influence of MgO on Young's modulus of silicate glasses. Studying the structure and elastic properties of $Na_2O{\cdot}MO{\cdot}4SiO_2$ glasses (M = Mg, Ca, Sr, Ba), Lin et al.[34] found reduced values of Young's modulus in glasses with M = Mg). They related this result to more abundant Q^4 species (three-dimensional SiO_4 network) besides the possible presence of silicate-rich/M-clusters interfaces. Pedone et al.,[30] investigating the effect of MgO (from 0.5 to 26.9 mol%) on 45S5 Bioglass have concluded that E decreased with the increase of MgO content, but the value reached a minimum for the glass with 10 mol% and increased again. Hand & Tadjiev[35] also observed lower values of E for silicate glasses with increased contents of MgO. However, they related this behavior to the small size of Mg that leads it to adopt a former network role instead of a modifier, increasing the network connectivity. However, it is essential to consider that Young's modulus close to those of cortical bone (7–25 GPa) is required to reduce the probability of implant failure due to the stress shielding phenomenon.[36] Although the values of E have been high compared to the cortical bone, we must keep in mind that this work can direct other studies with improved compositions or processing of the samples.

Changes in Ca^{2+}, Mg^{2+}, and P concentrations in SBF as a function of time are shown in Figure 3. Variations of Ca^{2+} and P contents in the solutions indicate competition between the consumption of these

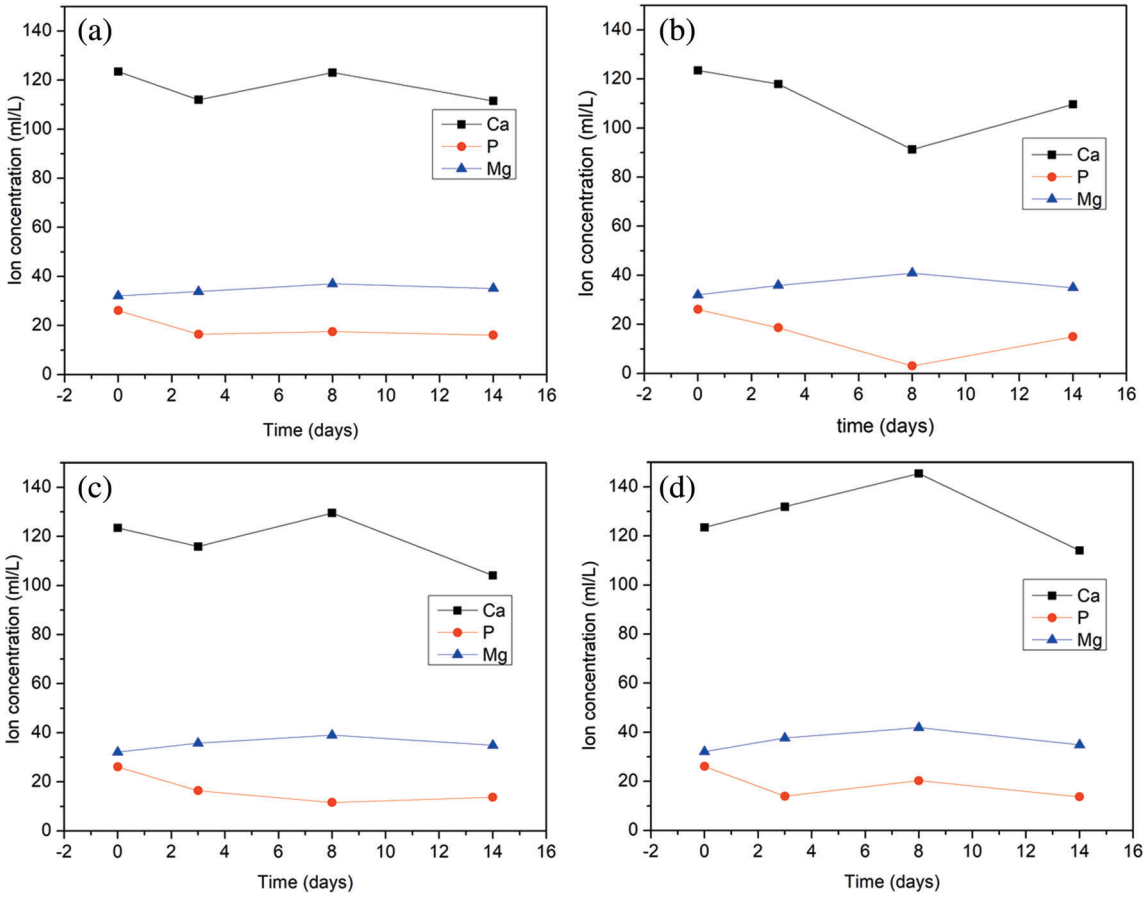

FIGURE 3 Variation of Ca^{2+}, Mg^{2+}, and P ions concentration in SBF after 2.5, 7.5, and 14 days of immersion of the (A) SN1, (B) SN2, (C) SN3, and (D) SN4 samples

ions to form the Ca–P surface layer and their release from the intergranular glass present in all samples. For SN1 and SN3 samples (Figure 3A,C), we can see that the Ca^{2+} ions into the solution were significantly reduced during the initial 2.5 days of immersion. After that, the content of these ions increased up to 7.5 days, followed by a reduction up to the 14th day. This last stage was more prominent for SN3 sample, showing the highest Ca-P layer growth rate. Still considering the same samples, it is possible to observe that the P concentration was initially reduced with a slight increase after 7.5 days for SN3.

For SN4 sample (Figure 3D), a rapid increase of Ca^{2+} ions concentration up to 7.5 days is observed, followed by their reduction. The release rate of Ca^{2+} ions from the intergranular phase was higher than the consumption rate from the SBF solution, owing to the high content of CaO in the sample composition (8 wt.%). Furthermore, although the phosphorus content has shown an initial reduction, its increase after 2.5 days suggests the dissolution of the Ca–P layer formed up to 7.5 days. On the other hand, SN2 sample (Figure 3B) promoted a significant Ca^{2+} and P ions consumption from SBF up to 7.5 days to form the Ca–P layer. After that, the increased concentration of these ions into the solution suggests a fast dissolution of the formed Ca–P layer.

The release of Mg^{2+} ions from the bioceramics to their respective solutions occurred up to 7.5 days of immersion. It increased with the increase in the content of MgO in the initial composition of the samples. However, from 7.5 to 14 days, the magnesium concentration in each solution was reduced, indicating its incorporation into the Ca–P layer.

Figure 4 illustrates SEM images of the studied samples after the immersions in SBF. According to this figure, it is clear that from 2.5 days of immersion onwards, particles are present on almost all samples. These results associated with those of ionic variation in SBF (Figure 3) indicate that such particles are crystals of Ca-P as a consequence of apatite nucleation on the surfaces. However, SN4 composition seems to have presented the ideal surface for apatite nucleation and growth up to day 2.5 of immersion (Figure 3M). This can be justified by the samples' porosity, which tends to assist in transporting ions from the intergranular vitreous phase towards the growing apatite crystals and the consequent high release rate of Ca^{2+} ions, shown in Figure 3D.

On day 7.5 (Figure 4B,F,J,N), it is evident that the number of apatite crystals was higher in SN4 sample, followed by SN3, SN1, and SN2, respectively. The slow apatite nucleation and growth processes in SN2, in this time, can be related due to its low porosity and high content of MgO, which led to the increased release of Mg^{2+} into the solution (Figure 3B).

From the 14th day, SN1 sample had a layer with scattered small crystals (Figure 4C). In contrast, on SN3 and SN4 (Figure 4K,O), a

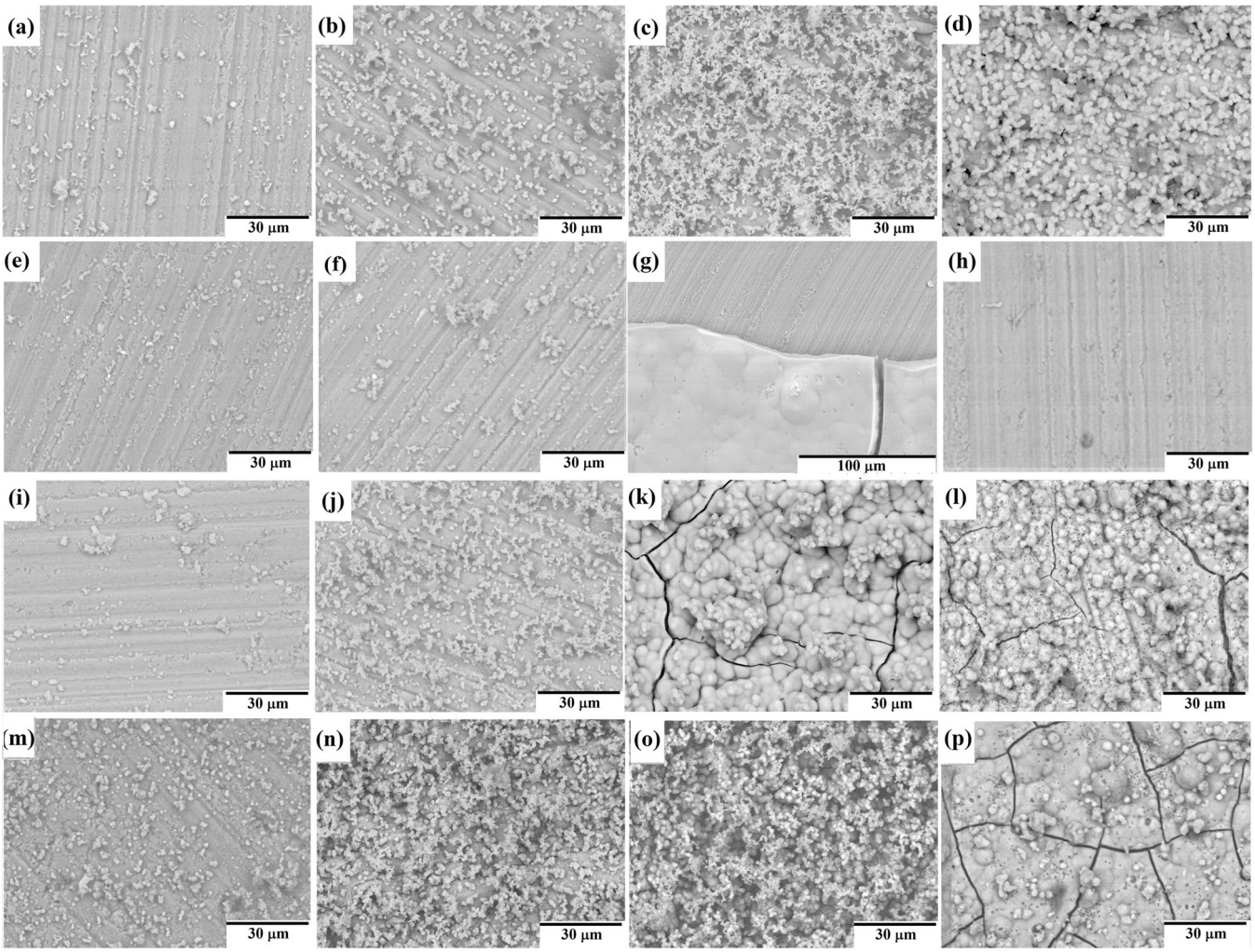

FIGURE 4 SEM images of the samples surfaces up to 24 days of immersion in SBF solution. (A) SN1/2.5 days, (B) SN1/7.5 days, (C) SN1/14 days, (D) SN1/24 days, (E) SN2/2.5 days, (F) SN2/7.5 days, (G) SN2/14 days, (H) SN2/24 days, (I) SN3/2.5 days, (J) SN3/7.5 days, (K) SN3/14 days, (L) SN3/24 days, (M) SN4/2.5 days, (N) SN4/7.5 days, (O) SN4/14 days, and (P) SN4/24 days

dense superficial film with numerous crystals with a spherical morphology typical of bone-like apatite was formed. Comparing SN3 and SN4 samples after 14 days of immersion, we can also notice that the highest apatite growth rate was found for SN3 sample, indicating its high reactivity over time, probably due to a more stable apatite layer which could continue to consume Ca^{2+} from SBF.

In addition, on the 14th day of immersion, SN2 sample (Figure 3G) had only part of its surface covered by a thick film (Figure 4G). On the 24th day (Figure 3H), the apatite layer has been completely dissolved or detached what is demonstrated by a surface morphology with no film or scattered particles (Figure 4H). These findings correlate well with the ICP analysis, which shows a significant increase of Ca^{2+} and P ions concentration into the solution after 7.5 days of immersion.

FEG-SEM images and EDS spectra of SN1, SN3, and SN4 samples after the 24th day of immersion in SBF (Figure 5) show that worn-like crystals, the morphology of hydroxyapatite at high magnification examination, form the globular aggregates containing Ca, P, Na, Mg, Si, and Cl. The Si peak is due to silicon nitride substrate while the presence of Ca and P peaks with high intensity indicates that the worn-like crystals are resulting from the calcium phosphate precipitation and have c ranging from 1.53 to 1.64 (Table 2). The atomic content ratios lower than 1.67 for hydroxyapatite can be associated with the occupation of some PO_4^{3-} sites by CO_3^{2-} and HPO_2^{4-} in the hydroxyapatite crystals, as observed by other works about apatite formed in SBF.[37] However, replacements of Ca^{2+} by Mg^{2+} can also contribute to the reduced Ca/P atomic ratios found here, as shown when we compared these values with those of (Ca + Mg)/P atomic ratios in Table 2. The presence of Na, Cl, and Mg suggests that these ions, from the SBF solution or additives composition, were incorporated into the calcium phosphate crystals.

The mechanism of apatite formation on the current samples can be compared to that on CaO–MgO–SiO_2 glasses since the intergranular glassy phase mainly contains CaO, MgO, and SiO_2.[38] This means that during the test, a hydrated silica gel layer was probably

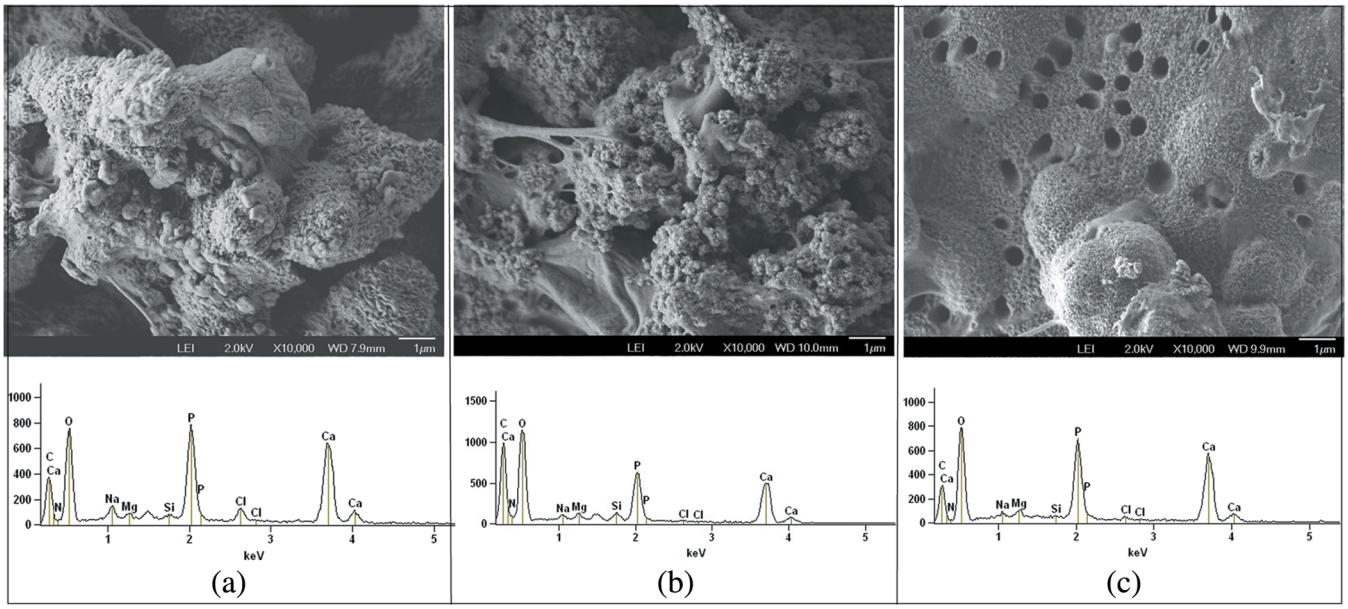

FIGURE 5 FEG images and EDS spectra of the samples surfaces after 24 days of immersion in SBF solution. (A) SN1, (B) SN3, and (C) SN4

TABLE 2 Ca/P and (Ca + Mg)/P ratios obtained using EDS analysis

Sample	Ca/P	(Ca + Mg)/P
SN1	1.64	1.68
SN3	1.50	1.59
SN4	1.53	1.61

firstly formed on the samples owing to exchanges of alkali or alkali-earth ions from their surfaces with H^+ and H_3O^+ ions from the SBF. As the newly silica gel layer acts as sites of nucleation and crystallization of apatite, it must have absorbed Ca^{2+} and PO_4^{3-} ions from the solution with subsequent formation of an amorphous calcium-phosphate layer that incorporates CO_3^{2-} and OH^- ions from SBF, forming bone-like HCA (hydroxycarbonate apatite).[39]

However, it has been reported that the formation and crystallization rates of the calcium phosphate layer on silicate glasses tend to be reduced with high MgO concentrations, which contributes to hinder the transformation of amorphous calcium phosphates to more stable apatite phases.[40] This can justify the low content of apatite crystals on SN2 sample surface on the 7th day of immersion in SBF and the partial and total absence of a film of apatite on the 14th and 24th days of immersion.

Besides the ceramic composition, another factor that contributes to the *in vitro* bioactivity is the surface morphology. Studies have demonstrated that rough and porous surfaces favor the crystallization of hydroxyapatite on Ca-containing bioactive glasses.[41] Eqtesadi et al.,[42] for example, observed that the presence of microporosity in robocasts of 13-93 scaffolds promotes better in vitro bioactivity than the same dense structures. Porosity tends to support the biomineralization process by accelerating the release of Ca^{2+} and PO_4^{3-} and their supersaturation levels around the environment.[43] This factor probably contributed to the high number of aggregates on SN4 porous sample on the first days of immersion in SBF and the dense superficial in the final days.

4 | CONCLUSIONS

In this article, different samples of silicon nitride ceramics with SiO_2, CaO, and MgO additions were obtained by pressureless sintering at 1750°C for 1 h under a nitrogen atmosphere. All studied compositions resulted in total $\alpha \rightarrow \beta$-Si_3N_4 transformation and developed a microstructure with needle-like grains dispersed in an intergranular phase. The densification behavior was affected by the combination and amounts of additives, that is, higher content of SiO_2 in the initial compositions were more able to form dense silicon nitride ceramics. In general, greater densification promoted higher values of fracture toughness, Young'modulus, and flexural strength. Still, the initial compositions also influenced the mechanical properties since lower SiO_2/MgO mass ratios tended to reduce the Young'modulus and hardness. SBF immersion tests demonstrated that the samples' bioactivity depends on the porosity and additives composition, with the mineralization ability achieved by samples with higher porosity and/or lower contents of MgO. Thus, the results indicate that an additive composition with high content of SiO_2 and CaO and low content of MgO may promote the formation of an apatite layer on silicon nitride ceramics after SBF immersion, as well as increased values of hardness, fracture toughness, and flexural strength. However, additional studies must be conducted performing some microstructural modifications to reduce the values of Young's modulus.

ACKNOWLEDGMENTS

The authors thank the Laboratory of Microscopy and Microanalysis and Laboratory of Chemical and Environmental Analysis of IPEN. This research was funded by Fundação de Amparo à Pesquisa do Estado de São Paulo, grant number 2015/02265-7.

DATA AVAILABILITY STATEMENT

The data that support the findings of this study are available from the corresponding author upon reasonable request.

ORCID

Celso Ricardo Sona Filho https://orcid.org/0000-0002-2051-9884

Flávio Machado de Souza Carvalho https://orcid.org/0000-0002-0238-4226

Cecilia Chaves Guedes-Silva https://orcid.org/0000-0002-3839-0839

REFERENCES

1. Guedes e Silva CC, Higa OZ, Bressiani JC. Cytotoxic evaluation of silicon nitride-based ceramics. *Mater Sci Eng*. 2004;*24*:643-646.
2. Guedes e Silva CC, König B Jr, Carbonari MJ, Yashimoto M, Allegrini S Jr, Bressiani JC. Tissue response around silicon nitride implants in rabbits. *J Biomed Mater Res A*. 2008;*84*:337-343.
3. Kersten RFMR, Wu G, Pouran B, et al. Comparison of polyetheretherketone versus silicon nitride intervertebral spinal spacers in a caprine model. *J Biomed Mater Res B Appl Biomater*. 2019;*107B*:688-699.
4. Calvert GC, Huffmon GV, Rambo WM Jr, Smith MW, McEntire BJ, Bal BS. Clinical outcomes for lumbar fusion using silicon nitride versus other biomaterials. *J Spine Surg*. 2020;*6*:33-48.
5. Özmen Y. Si_3N_4 as a biomaterial and its tribo-characterization under water lubrication. *Lubr Sci*. 2016;*28*:243-254.
6. Rondinella A, Marin E, Zanocco M, Boschetto F, Pezzotti G. Surface pre-oxidation improves the wear performance of Si_3N_4 against UHMWPE. *Appl Surf Sci*. 2019;*1*:1037-1045.
7. Frajkorová F, Bodisová K, Bohác M, Baronicková E, Sedlácek J. Preparation and characterisation of porous composite biomaterials based on silicon nitride and bioglass. *Ceram Int*. 2015;*41*:9770-9778.
8. Fu L, Xiong Y, Carlsson G, et al. Biodegradable Si_3N_4 bioceramic sintered with Sr, Mg and Si for spinal fusion: surface characterization and biological evaluation. *Appl Mater Today*. 2018;*12*:260-275.
9. Wananuruksawong R, Wasanapiarnpong T, Dhanesua N, Didron PP. Microhardness and biocompatibility of silicon nitride ceramic developed for dental applications. *Mater Sci Appl*. 2014;*5*:1034-1039.
10. Xu Z, Wu H, Wang F, et al. A hierarchical nanostructural coating of amorphous silicon nitride on polyetheretherketone with antibacterial activity and promoting responses of rBMSCs for orthopedic applications. *J Mater Chem B*. 2019;*9*:1-26.
11. Precnerová M, Bodi K, Galusková D. In vitro bioactivity of silicon nitride: hydroxyapatite composites. *Ceram Int*. 2015;*41*:8100-8108.
12. Usinskas P, Stankeviciute Z, Niaura G, et al. Sol–gel processing of calcium hydroxyapatite thin films on silicon nitride (Si_3N_4) substrate. *J Sol-Gel Sci Technol*. 2017;*83*:268-274.
13. Guedes-Silva CC, Rigo ECS, Marchi J, Bressiani AHA, Bressiani JC. Hydroxyapatite coating on silicon nitride surfaces using the biomimetic method. *Mater Res*. 2008;*11*:47-50.
14. Ziegler G, Heinrich J, Wotting G. Review: relationships between processing, microstructure and properties of dense and reaction-bonded silicon nitride. *J Mater Sci*. 1987;*22*:3041-3086.
15. Guedes-Silva CC, Carvalho FMS, Bressiani JC. Effect of rare-earth oxides on properties of silicon nitride obtained by normal sintering and sinter-HIP. *J Rare Earths*. 2012;*30*:1177-1183.
16. Lu HH, Huang JL. Effect of Y_2O_3 and Yb_2O_3 on the microstructure and mechanical properties of silicon nitride. *Ceram Int*. 2001;*27*:621-628.
17. Ling G, Yang H. Pressureless sintering of silicon nitride with magnesia and yttria. *Mater Chem Phys*. 2005;*90*:31-347.
18. Han W, Li Y, Chen G, Yang Q. Effect of sintering additive composition on microstructure and mechanical properties of silicon nitride. *Mater Sci Eng A*. 2017;*700*:19-24.
19. Guedes-Silva CC, Rodas ACD, Silva AC, et al. Microstructure, mechanical properties and in vitro biological behavior of silicon nitride ceramics. *Mater Res*. 2018;*21*:e20180266.
20. Guedes-Silva CC, Rodas ACD, Carvalho FMS, Higa OZ, Ferreira TS. Silicon nitride with titania, calcia and silica additives for orthopaedic applications. *Process Appl Ceram*. 2020;*14*:63-70.
21. Henstock JR, Canham LT, Anderson SI. Silicon: the evolution of its use in biomaterials. *Acta Biomater*. 2015;*11*:17-26.
22. Jeong J, Kim JH, Hwang NS, Heo CY. Bioactive calcium phosphate materials and applications in bone regeneration. *Biomater Res*. 2019;*23*:1-11.
23. Liu C, Ren Z, Xu Y, Pang S, Zhao X, Zhao Y. Biodegradable magnesium alloys developed as bone repair materials: a review. *Scanning*. 2018;*2018*:1-15.
24. Bellucci D, Sola A, Salvatori R, Anesi A, Chiarini L, Cannillo V. Role of magnesium oxide and strontium oxide as modifiers in silicate-based bioactive glasses: effects on thermal behavior, mechanical properties and in-vitro bioactivity. *Mater Sci Eng C*. 2017;*72*:566-575.
25. ASTM: American Society for Testing Materials. ASTM E 1876-01: standard test method for dynamic Young's modulus, shear modulus, and Poisson's ratio by impulse excitation of vibration. West Conshohocken, p. 1–16. 2005.
26. ASTM: American Society for Testing Materials. ASTM C 1161-13: standard test method for flexural strength of advanced ceramics at ambient temperature. West Conshohocken, p. 1–19. 2013.
27. Anstis GR, Chantikul P, Lawn BR, Marshall DB. A critical evaluation of indentation techniques for measuring fracture toughness. Indirect crack measurements. *J Am Ceram Soc*. 1981;*62*:535-538.
28. Hampshire S, Drew RAL, Jack KH. Oxynitride glasses. *Phys Chem Glasses*. 1985;*26*:182-186.
29. Park JH, Lakes RS. Structure-property relationship of CaO–MgO–SiO_2 slag: quantitative analysis of Raman spectra. *Metall Mater Trans B*. 2013;*44*:938-947.
30. Pedone A, Malavasi G, Menziani MC, Segre U, Cormack AN. Role of magnesium in soda-lime glasses: insight into structural, transport, and mechanical properties through computer simulations. *J Phys Chem C*. 2008;*112*:11034-11041.
31. Hallab NJ, Cunningham BW, Jacobs JJ. Spinal implant debris-induced osteolysis. *Spine*. 2003;*28*:S125-S138.
32. Vallet-Regí V, Salinas AJ, Roman J, Gil M. Effect of magnesium content on the in vitro bioactivity of CaO–MgO–SiO_2–P_2O_5 sol-gel glasses. *J Mater Chem*. 1999;*9*:515-518.
33. Chen X, Ou J, Wei Y, Huang Z, Kang Y, Yin G. Effect of MgO contents on the mechanical properties and biological performances of bioceramics in the MgO–CaO–SiO_2 system. *J Mater Sci Mater Med*. 2010;*21*:1463-1471.
34. Lin CC, Chen SF, Liu L, Li CC. Size effects of modifying cations on the structure and elastic properties of Na_2O–MO–SiO_2 glasses (M = Mg, Ca, Sr, Ba). *Mat Chem Phys*. 2010;*123*:569-580.
35. Hand RJ, Tadjiev DR. Mechanical properties of silicate glasses as a function of composition. *J Non-Cryst Solid*. 2010;*356*:2417-2423.
36. Faber KT, Evans AG. Crack deflection process: I. Theory. *Acta Metall*. 1983;*31*:465-576.

37. Cheng Y, Liu P, Xiao P, et al. Effect of surface chemical modifications on the bioactivity of carbon fibers reinforced epoxy composites. *Surface Coat Technol*. 2019;*377*:124889.
38. Ni S, Chang J, Chou L. *In vitro* studies of novel CaO–SiO_2–MgO system composite bioceramics. *J Mater Sci Mater Med*. 2008;*19*:359-367.
39. Huang M, Zhang M, Yao D, et al. Dissolution behavior of CaO–MgO–SiO_2-based bioceramic powders in simulated physiological environments. *Ceram Int*. 2017;*43*:9583-9592.
40. Chen X, Liao X, Huang Z, et al. Synthesis and characterization of novel multiphase bioactive glass-ceramics in the CaO–MgO–SiO_2 system. *J Biomed Mat Res B: App Biomat*. 2010;*93*:194-202.
41. Cannillo V, Pierli F, Ronchetti I, Siligardi C, Zaffe D. Chemical durability and microstructural analysis of glasses soaked in water and in biological fluids. *Ceram Int*. 2009;*35*:2853-2869.
42. Eqtesadi S, Motealleh A, Pajares A, Miranda P. Effect of milling media on processing and performance of 13-93 bioactive glass scaffolds fabricated by robocasting. *Ceram Int*. 2015;*41*:1379-1389.
43. Zhang K, Fan Y, Dunne N, Li X. Effect of microporosity on scaffolds for bone tissue engineering. *Regen Biomat*. 2018;*5*:115-124.

How to cite this article: Sona Filho, C. R., Machado de Souza Carvalho, F., & Chaves Guedes-Silva, C. (2022). Mechanical properties and *in vitro* bioactivity of silicon nitride ceramics with SiO_2, CaO, and MgO additions. *Journal of Biomedical Materials Research Part B: Applied Biomaterials*, *110*(3), 507–516. https://doi.org/10.1002/jbm.b.34930